Published in final edited form as:
Nanotechnology. 2010 June 4; 21(22): 225102. doi:10.1088/0957-4484/21/22/225102.

Generation and detection of plasmonic nanobubbles in zebrafish

E Y Lukianova-Hleb[1,2], **C Santiago**[1], **D S Wagner**[1], **J H Hafner**[1], and **D O Lapotko**[1,2]

[1] Rice University, 6100 Main Street, TX 77005, USA

[2] A V Lykov Heat and Mass Transfer Institute, 15 P Brovka Street, Minsk, 220072, Belarus

Abstract

The zebrafish embryo has been evaluated as an *in vivo* model for plasmonic nanobubble (PNB) generation and detection at nanoscale. The embryo is easily observed and manipulated utilizing the same methodology as for application of PNBs *in vitro*. Injection and irradiation of gold nanoparticles with a short laser pulse resulted in generation of PNBs in zebrafish with similar parameters as for PNBs generated in water and cultured living cells. These PNBs do not result in systemic damage, thus we demonstrated an *in vivo* model for rapid and precise testing of plasmonic nanotechnologies.

1. Introduction

Development of diagnostic and therapeutic methods and materials based on plasmon resonance includes an important stage of *in vivo* verification and evaluation. This often creates the biggest challenge for plasmonic technologies when standard animal models are employed [1–9]. Few animal models provide the optical clarity and ease of observation provided by the cell culture *in vitro* models that are used for the initial characterization of plasmonic diagnostic and therapeutic effects. Due to their large size and internal development, mammalian model organisms are not well suited for precise control of the nanoparticles (NP) and plasmonic NP-induced processes: optical activation and detection are compromised (and sometimes suppressed) by the optical scattering and absorption properties of tissues; it is difficult to control the distribution of the NPs in real time and monitor plasmonic interactions in a large opaque animal host [10–14]. Due to these imaging and delivery challenges, cellular and molecular resolution (where the bio-effects of NPs occur) may not be available for non-invasive studies. Together, these challenges limit the efficacy and accuracy of controlling and observing plasmonic effects and developing *in vivo* plasmonic nanomedicine.

Our aim was to develop an efficient *in vivo* model for plasmonic diagnostic, therapeutic and theranostic (combined diagnosis and therapy) methods by using zebrafish. Zebrafish are vertebrate organisms that are relatively optically transparent, develop quite fast and are physiologically similar to human. Zebrafish have already been evaluated for analysis of the distribution and toxicity of plasmonic (gold) NPs [15–17] and have also allowed efficient optical manipulations including laser microsurgery and sensing [18–22]. These findings allowed us to consider zebrafish embryos for plasmonic nanomedicine (optical scattering diagnosis, photothermal diagnosis and therapy, ultrasound and optical methods for drug delivery, cell manipulation and surgery). Furthermore, the zebrafish is a model for diverse cancers [23–28], which are targets for plasmonic therapies. Therefore, zebrafish have an

dmitri.lapotko@rice.edu .

excellent potential for nanophotonic medicine. Based on these already established properties of zebrafish (ease of culture, optical transparency, low gold toxicity and cancer models) we have hypothesized that zebrafish can be used as an efficient *in vivo* model for cell level plasmonic nanotechnologies for diagnosis, therapy and theranostics. We tested this hypothesis experimentally by focusing on two tasks: by generating and detecting therapeutic and diagnostic plasmonic processes around gold NPs in living zebrafish, and on the safety of NP targeting, activation and detection. We have used a single short laser pulse excitation of transient and localized vapor nanobubbles (defined by us as plasmonic nanobubbles—PNB) around gold NPs [29] (figure 1). This mode of plasmonic interaction has been previously shown in cultured cells to provide a single cell selectivity of therapeutic (mechanical) effect of bubble generation [30,31] without producing a thermal impact to surrounding cells [32]. The sensitivity of optical scattering imaging of PNBs is 10–100 times higher than the sensitivity of gold NP scattering methods [33,34]. Most important, plasmonic nanobubbles have been shown to be tunable probes whose properties can be dynamically tuned from non-invasive to damaging modes by the fluence of the pump laser pulse [35]. These features indicate a high diagnostic and therapeutic potential of PNBs that needs adequate *in vivo* testing in model organisms for the development of transformative technologies. In this work we have developed a novel *in vivo* zebrafish-model so as to evaluate the potential for optical generation and detection (imaging) of plasmonic nanobubbles *in vivo*.

2. Materials and methods

2.1. Plasmonic nanobubbles (PNB): optical generation and detection

PNBs were generated by laser pulse-heating of gold NPs. Evaporation of the medium around an NP involves several processes: laser pulse-induced thermalization of a NP occurs in approximately 1 ps [36]; thermal diffusion from a NP to the adjoining medium forms a thin vapor layer around a NP; when the pressure inside vapor layer exceeds the surface tension pressure the vapor bubble begins to expand to a maximal diameter and then collapses. The bubble lifetime may be considered as proportional to its maximal diameter [37–39] and thus can be used as a measure of the bubble size and of its mechanical action (which is associated with the bubble expansion and collapse). Such vapor bubbles use the plasmon resonance mechanism as a heat source and their size can be tuned at nanoscale by varying the fluence of pump laser pulse [29]. To distinguish these bubbles from other phenomena we have defined them as plasmonic nanobubbles. The minimal fluence of a single laser pulse that provides bubble generation is defined as the PNB threshold fluence. It was experimentally measured as the fluence that provides the generation of PNBs in 50% of the cases of exposure to individual laser pulses. When the optical pulse duration is less than the thermal relaxation time, the losses due to thermal diffusion are negligible, and the entire heat released is concentrated in a small volume around the heat source. In our work we have employed a pulse of length 0.5 ns, 532 nm (STA-01 SH, Standa Ltd, Vilnius). The pump laser beam was directed into the illumination path of an inverted optical microscope and was focused into the sample. The laser beam diameter was 14 μm in the sample plane. Single events were studied.

PNB detection has been realized with two optical methods that take advantage of the excellent optical scattering properties of bubbles [40]. We previously developed these methods for the imaging of the photothermal phenomena in living cells with the pump–probe laser microscope [33,41]. The time-resolved imaging of NPs and PNBs was realized by using side illumination of the sample with a custom made pulsed probe dye laser beam at a wavelength (690 nm, 0.5 ns, dye laser) and with a tunable time delay of 1–10 ns relative to the pump pulse (figure 2). The scattered probe radiation was imaged with a digital camera (Luka, Andor Technologies, Ireland). For quantitative analysis of the optical amplification we have employed differential images: $S_{sc}(t) = [I(t) - I_b]$ that describes the pixel image

amplitude *I*(t) of optical scattering by a transient PNB and compensates for the stationary scattering from the background (cell, tissue). While allowing us to image and quantify the PNB the pulsed imaging can hardly provide kinetic measurement. The latter was realized by the thermal lens method in a response mode. An additional continuous probe beam (633 nm) was directed at the sample and focused on it collinearly with the probe laser beam and its scattered by PNB component was monitored by a high-speed photodetector (PDA510, Thorlabs Inc.). The response mode allowed measurement of the PNB lifetime that characterizes the maximal diameter of the bubble. Image and response modes were used simultaneously, thus combining the imaging and measuring of the lifetime (figure 2). An additional pulsed laser (532 nm, 10 ns, LS 2132 by Lotis TII, Minsk) was used for the excitation of red fluorescence from ethidium bromide dye. The fluence of this laser was set at a level well below the PNB generation threshold (which is quite high for such long pulses).

2.2. Experimental models and samples

2.2.1. Nanoparticles—We have used conjugates of 60 nm gold spheres with anti-epidermal growth factor receptor (EGFR) antibody C225 that were obtained from Nanopartz Inc. (Salt Lake City, UT). The nanoparticles were fabricated with a surface chemistry that prevented their spontaneous aggregation. The plasmon resonance wavelength of such a NP is very close to 532 nm as has been verified with optical spectroscopy of the NP suspension. Water samples of the nanoparticles were prepared in standard 9 mm culture wells (#C24765, Molecular Probes, Inc., Eugene, OR). NP clusters are groups of 10–50 aggregated NPs. Such clusters were prepared by adding 0.9% NaCl to the NP suspension (dilution 1:10). Formation of the clusters has been verified by two methods: by electron microscopy and optical spectroscopy. The latter has shown typical broadening of the extinction spectrum while maintaining significant absorption at 532 nm.

2.2.2. Zebrafish—Zebrafish were maintained in accordance with protocols approved by the Rice University Institutional Animal Care and Use Committee. Zebrafish were maintained at 28 °C in recirculating water systems (Aquatic Habitats) in 14 h light 10 h dark. Zebrafish embryos were obtained from natural matings of wild type parents. 30 h post fertilization embryos (hpf) were imbedded in 1% low melt agarose (#A-9045, Sigma-Aldrich Corp., St Louis, MO). 4 nl of 2.6×10^{10} particles ml^{-1} was injected subcutaneously into the flank at the level of the end of the yolk extension. Successful injection was monitored by local inflation of the skin. Since the mechanisms of nanoparticle bio-distribution are complex we did not consider them in the current work and have focused on the evaluation of PNBs in zebrafish and around locally injected NPs. Embryos were removed from low melt agarose and placed in embryo medium (E3) in bridged coverslips [42]. Injected embryos and mounted uninjected embryos were subjected to PNB induction in multiple locations around and distant to the injection site. Embryos were removed from the bridged coverslip and monitored for survival. Injected PNB-induced embryos survived to nine days post fertilization, developed swim bladders and showed no obvious defects associated with treatment.

2.2.3. Cells—For the tissue culture based *in vitro* experimental model we have used the same gold spheres resuspended in cell culture media RPMI-1640 (Sigma, St Louis, MO). The cells were prepared as monolayers of living isolated lung carcinoma cells (A549) that were obtained from ATCC and were grown into standard 9 mm culture wells (#C24765, Molecular Probes, Inc., Eugene, OR). All cells were incubated with NPs for 60 min at 37 °C. The concentration of the NPs during the incubation was adjusted to $0.2–0.9 \times 10^{11}$ ml^{-1}. During non-specific endocytosis the NPs were internalized and concentrated into clusters of closely packed NPs in endosomal compartments, as we have shown earlier [31,43,44]. Cell

viability was evaluated optically using two standard microscopy techniques. First, a bright light image was obtained for the cell before and after its exposure to the pump pulse and the difference of these two images was used to detect any PNB-induced changes of the shape of the cell, in particular, emerging of the blebbing bodies. Blebbing bodies may develop in the cells with damaged cytoskeleton and even with an intact membrane. Second, the membrane damage by PNB was detected using a standard fluorescent method by monitoring the cellular uptake of ethidium bromide (EtBr) dye. Fluorescent images were obtained for each cell before and after their exposure to the pump laser pulses. Any significant increase of the EtBr-specific fluorescence observed 60 s after the pump laser pulse is considered as the sign of the membrane disruption, and such cell was classified as the damaged. Although these methods did not provide the monitoring of the long term viability, they can be applied on site and to specific individual cells during the generation of the PNBs and without removing the cells from the sample chamber.

3. Results and discussion

We tested PNB generation in an aqueous suspension of gold NPs, within tissue culture cells and within one day post fertilization (dpf) zebrafish embryos. To provide a basis for the studies of PNBs in zebrafish embryos we have initially generated and detected PNBs under the most controllable conditions: in water suspension of identical gold NPs and their clusters (figure 3). Optical scattering by the PNB has been detected as a time resolved image (figure 3(b)) and a time-response (figure 3(a)). PNB generation has been studied by us previously and the details regarding the physical, thermal and optical properties of the PNB can be found in our recent work [29,32,34]. First, we determined the PNB generation threshold fluence of a 532 nm 0.5 ns laser pulse for single NPs using 60 nm gold spheres in water. The threshold was found to be 110 mJ cm^{-2} for the fluence that provides 0.5 probability of PNB generation. For the NP clusters the PNB threshold has been found to be significantly lower: 70 mJ cm^{-2}. We have shown previously that NP clusters allow us to decrease the bubble generation fluence of the pump laser pulse and thus to decrease the laser-induced thermal load on the tissue. Furthermore, under decreased laser fluence the PNBs were selectively generated only around the NP clusters while single NPs did not yield bubbles at such a fluence level. Next, we measured optical scattering image amplitudes and lifetimes for the PNBs that were generated around isolated single 60 nm gold spheres and their clusters under a pump laser pulse fluence of 200 mJ cm^{-2} (which is well above the PNB generation threshold fluence). Single laser pulses were applied (table 1). The lifetime of the PNB characterizes its maximal diameter (which can be expected to be in submicrometer range for this fluence) and can be considered as a quantitative measure of the mechanical action of the PNB. Optical scattering image amplitudes were also averaged so as to characterize the sensitivity of the PNB as an optical probe (table 1). Compared to gold NPs, the PNBs amplified optical scattering by up to 20 times. Also, the NP clusters produced bigger bubbles compared to those generated around single NPs. The parameters obtained for the PNB generation and detection were then employed for *in vitro* and *in vivo* experiments.

A549 lung carcinoma cells were incubated for 60 min at 37 °C with the same gold NPs as were used in the above experiments. Then individual cells were irradiated with single pump laser pulses at various fluence levels. We measured the PNB generation threshold fluence, the dependence of the PNB lifetime and scattering image amplitude upon the pump laser fluence, and the viability of the cells after their exposure to the laser pulse (with 60 s delay). For each cell we registered bright field and side scattering optical images before and after the pump laser pulse (figure 4). The lifetime of PNBs detected in the cells under the pump laser fluence of 200 mJ cm^{-2} was 50 ± 21 ns (table 1), which was longer than that for individual NPs under the same laser fluence. The amplitudes of PNB scattering images obtained at this fluence were close to those obtained for NP clusters in water (table 1).

Furthermore, the PNB threshold fluence as measured for the NP-treated cells (table 2) was found to be lower than the PNB generation threshold for single NPs (110 mJ cm^{-2}). These results allowed us to conclude that the PNBs were generated in cells around NP clusters and not around single NPs.

Optical scattering amplitudes of the PNBs were compared to those for gold NPs in the cells (without exposure to pump laser pulse). According to table 1 the PNBs have significantly amplified optical scattering of gold NPs, thus improving the sensitivity of PNB as optical probes by more than one order of magnitude relative to NPs.

Detection of cell damage was based on the uptake of a fluorescent cell impermeant dye, ethidium bromide, and additionally, on observation of blebbing bodies in bright field images of the cells after the pulse (figure 4(c)). A dye-specific signal was detected within 60 s after the treatment of cells with a single laser pulse and the accompanying PNB.

We found that the degree of cell damage was correlated to the level of the pump laser fluence and to the PNB lifetime (table 2): cells were not damaged by pump laser pulses with fluences below 1.0 Jcm^{-2} or by the corresponding PNBs with lifetimes below 110 ns. Thus the PNB generation threshold in living cells was almost ten times lower than the cell damage threshold fluence. Since the PNB lifetime is determined by the maximal size of the PNB and depends linearly on the fluence of the pump laser pulse [37–39], we may assume that the observed laser-induced damage of the cells was related to the PNB size. Small (short lifetime) PNBs generated at low fluence did not damage the cells, while bigger (relatively long lifetime) PNBs were associated with damage to the cell membrane. It should be noted that such damage was quite local since the collateral cell that produced no detectible PNBs was not damaged (figure 4(c)). The viability of the adjacent cell was also verified by the absence of ethidium bromide fluorescence (unlike in the neighboring cell that yielded the PNBs and later produced a damage-specific fluorescence). Laser-induced bubbles were also observed in untreated cells. In this case the bubbles might have been generated due to optical absorption by endogenous chromophores and follow up heating. Generation of bubbles in untreated cells has always coincided with their damage (table 2) and such bubbles could not be tuned as we demonstrated for PNBs.

We applied the aqueous and cell culture PNB methods to the zebrafish and determined the optical and mechanical properties of PNBs *in vivo*. We injected 60 nm gold nanospheres into the flank of one day post fertilization embryos. We irradiated the embryos with the same single short laser pulses (532 nm, 0.5 ns, 200 mJ cm^{-2}) on the same apparatus that we used to generate PNBs *in vitro*. We irradiated several points located inside and outside the NP injection area (figure 5(a)). We registered bright field and side scattering images of each point prior to their exposure to the pump laser pulse. Next, we recorded the side scattering image of the same area with a 10 ns time delay relative to the pump pulse and subtracted the previous scattering image. The resulting differential image (figure 5(b)-I, II) clearly showed PNBs, which also had a time response signal with a shape typical for PNBs (figure 5(d)-I, II). PNBs were detected only within the injection area while no PNBs were detected outside this area (figures 5 III-((b), (d))). The lifetimes of the PNBs among the sampled points (inside injection area) varied between 20 and 700 ns at a fixed laser pulse fluence of 200 mJ cm^{-2} (table 1). This range corresponds to the PNB lifetime observed for single NPs at the low end and NP clusters at the high end; these yield much longer PNBs (table 1). Therefore, the PNBs detected in zebrafish show the same response as we observe from cultured cells and water suspension models and are generated by single NPs (figure 5(d)-II) and by their clusters (figure 5(d)-I) (depending upon the actual aggregation state of the NPs after their injection).

Optical scattering images related to the PNBs were also detected only within the injection area. PNB-related amplitude in the light scattering images were well above the tissue-generated background scattering (figure 5(c)-III, table 1), while the scattering from the corresponding NPs (without their exposure to the pump laser pulse) was weaker or comparable to the tissue scattering and did not exceed the background scattering (figure 5(c), table 1). Therefore, PNBs as optical probes were much brighter than NPs, and were detectable in living tissue under conditions when the NPs could not been detected due to the strong background scattering.

Data from each model are presented in table 1 to compare the mechanical (through the PNB lifetimes) and optical (through the scattering image amplitudes) properties of PNB generated *in vivo*, in cultured cells and in water suspension of gold NPs. In all three groups we have used identical NPs and optical excitation and detection conditions and schemes. This justifies the direct comparison of the data obtained for totally different samples. Analysis of the PNB lifetimes indicated that *in vivo* and *in vitro* generated PNBs are likely to be generated by NP clusters that may form in cells and after the injection in zebrafish. The level of optical scattering amplitudes for the *in vivo* and *in vitro* generated PNBs were close to each other and their level also corresponded to NP clusters rather than to single NPs (figure 5(c)). Therefore, we may suggest that the signals observed in NP-treated zebrafish were associated with the generation of plasmonic nanobubbles around clusters of gold NPs and were not accompanied by thermal effects such as hyperthermia. The mechanism of NP clusterization in living cells has been studied by us earlier for *in vitro* cell models [43,44] but requires additional studies for the *in vivo* model. This is the subject of future work that will employ the optical transparency of zebrafish to image and monitor the NPs and their local and systemic effects.

No large scale tissue disruption or alteration has been detected in bright field images of the zebrafish after generating the PNBs. The viability of each individual specimen was monitored until 9 dpf and is summarized in table 3. We used several control samples so to exclude the possible influence of the preparation steps on the viability. Each group in table 2 was counted from 2 to 9 identical zebrafish. With one exception for a NP injection control all other experimental stages (including laser treatment and the generation of PNBs) did not cause any lethality. Therefore, generation and detection of plasmonic nanobubbles by itself is not lethal. This observation provides us with wide opportunities for using zebrafish as an *in vivo* platform for evaluating diagnostic and therapeutic methods based on plasmonic interactions.

Most NP studies *in vivo* are related to nanotoxicology and rely upon the analysis of the bio-distribution of gold NPs in animals. Plasmonic NPs and mediated effects have been extensively studied *in vivo* with standard animal models (usually mouse and rat). Several methods employed included inductively coupled plasma-mass spectrometry (measures the mass of gold in a tissue sample [2–4]), electron microscopy (directly shows the location of individual NPs or their clusters in tissue [2]), the methods of histopathology [6] and of coherent anti-Stoke Raman scattering microscopy [9] (allow optical detection of gold NPs in tissues as well as the tissue response to exposure to NPs). All these methods require the extraction of the tissue samples from an animal and a long preparation procedure. Based on the results obtained for zebrafish (see above and also [15–17]) we may suggest that in some cases the bio-distribution of gold NPs in zebrafish can be analyzed with PNB methods in a non-invasive and real time manner.

Several methods of optical and opto-acoustic sensing and imaging have been evaluated *in vivo* with the purpose of the development of diagnostic applications. Two-photon luminescence provided imaging of nanoparticles with near-infrared plasmon resonances, in

particular, single gold nanorods were imaged *in vivo* using this technique [1]. The reported signal-to-noise (background) ratio was about 3 while our results have indicated a signal-to-background ratio of PNB imaging about 9 for single NPs and more than 10 for NP clusters (table 1). Therefore, PNB imaging may provide better sensitivity *in vivo* comparing to the two-photon methods. Furthermore, PNB imaging can be achieved with any type of the NPs and does not require a specific wavelength (as for the two-photon method). Another method uses surface-enhanced Raman scattering (SERS) [2] and detects specific molecular signatures *in vivo* with near-infrared excitation from subcutaneous and deep (1 cm) tissues. This method depends upon acquisition of spectral data with high precision and sensitivity, which requires a relatively long (>1 s) integration time, while PNB sensing is much faster (10 ns) and allows more flexibility in technical realization. Diffuse optical spectroscopy [8] has been applied for the detection of gold nanoshells with the signal-to-background ratio being approximately 2 (based on the amplitudes of reflectance signals before and after NP injection) and with a subsecond collection time. Opto-acoustic imaging methods have also reported a centimeter range but cannot detect individual NPs or individual cells and generally have lower sensitivity and specificity compared to the above optical methods.

All optical methods depend upon optical transparency of the object and, therefore, are limited by the depth of penetration of optical radiation into tissues, with the maximum reported range of 1 cm, because the tissues in employed animal models were not transparent. Zebrafish eliminate this limitation due to their optical transparency and allow real time access to individual cells. Furthermore, our results have shown that the delivery and collection of optical radiation to/from zebrafish is much simpler compared to the schemes employed in the cited studies with mice and rats. With the exception of two-photon luminescence [1] the optical methods considered above cannot detect single NPs, whereas PNB imaging of zebrafish can detect single NPs and discriminate between single NPs and clusters (table 1). The speed of NP detection and imaging is an important parameter since the plasmonic interactions occur at a cellular and molecular level. Single pulse PNB imaging requires 10 ns to obtain the image, which is much faster than any reported method. Adding the high sensitivity and non-invasive nature of small PNBs this method may provide real time sensing and imaging of single NPs or their clusters, and without damage to the host animal. Therefore, we may conclude that using zebrafish may improve the accuracy and efficacy of *in vivo* evaluation of the NP-based diagnostic methods.

One potential limitation to this technology is the generation of bubbles around endogenous biomolecules. To examine bubble generation in zebrafish embryos that do not contain NPs, we tested the ability of two different tissues to generate photothermal bubbles at fluences far above those required for PNB generation in embryos containing gold NPs. A single pump laser pulse was been directed into the tail muscle and the axial blood vessels (figures 6(a) and (e)). Application of the pulse at the same fluence of 200 mJ cm^{-2} returned no signal (table 1) or any detectible alteration in the bright field image of the irradiated area. The increase of the fluence up to 500 mJ cm^{-2} also resulted in no bubbles (figures 6(b) and (c)) or optically detectible damage to the tissues (figure 6(d)). However, the latter fluence level has caused transient heating of the blood vessels, as was observed though the heating-specific shape of the time response (not shown). Bubbles were detected after increasing the pump laser fluence to 740 mJ cm^{-2} (figures 6(f) and (g)). These bubbles were characterized by a relatively long lifetime (above 500 ns) and were also accompanied by oscillations and environmental heating of the irradiated zone (compare figure 5(c)-I, II and figure 6(g)). The observed heating and bubbles were naturally caused by the optical absorption of pump laser pulse by the hemoglobin in red blood cells, since the exposure of other types of tissue did not result in any detectible signals at all. The mechanism of the hemoglobin-generated bubbles is different from that for plasmonic nanobubbles: the size of the red blood cell is almost 1000 times larger and the heat is generated as a result of non-radiational relaxation of

hemoglobin molecules and not through the interaction of free electrons with phonons, as in a case of plasmonic NP. Such relatively large photothermal bubbles also disrupted collateral tissues (figure 6(h)). Thus, endogenous bubbles were generated only under strong illumination and these bubbles had different properties from the PNBs.

Detailed analysis of the PNB time responses obtained for aqueous samples, cultured cells and zebrafish, showed that after the PNB collapse no residual heating of the environment occurs because the signal level after the PNB collapse was equal to the baseline (figures 3(a), 4(d), 5(d)-I,II). This physical effect is associated with the thermal insulation properties of PNB and has been studied in detail by us previously [29, 32]. This property is opposite to the NP-induced hyperthermia that is used more widely. NP-induced hyperthermia is usually achieved with a long optical excitation of several minutes, not a single pulse as in our method. More NPs are required so to provide the heating of a bulk volume that is much larger than that of the single NP. We have not detected any thermal impact from a single laser pulse so we may conclude that the PNB mechanism of cell damage is related to the mechanical and highly localized action of the bubble, whose rapid expansion above a critical diameter (estimated as approximately 2 μm) disrupts cellular components such as cytoskeleton and membrane. This mechanism is in line with the fast (less than a minute) observed disruption of the membrane and with the rapid (2–3 min) appearance of blebbing bodies in the cells (figure 4(c)). Unlike the thermal field around NPs (which is responsible for thermal damage induced with continuous lasers) or a NP-induced pressure wave (which is responsible for mechanical damage induced with pulsed lasers), the single PNB-induced damage was found to be cell-specific because we have never observed damage to the collateral cells if those cells have generated no bubbles. Therefore, among all optical processes, the NP-generated nanobubbles provide the most localized and controllable therapeutic action of a mechanical nature and at the same time act as very sensitive optical probes.

Therapeutic applications of plasmonic NPs *in vivo* mainly employ the drug delivery and thermal effects of NP optical activation. Both applications rely on the selectivity of NP targeting and on precise control of the optical energy that is delivered to the NPs. The direct therapeutic action of plasmonic NPs has been reported through several mechanisms. The thermal effect of plasmon resonance is the most recognized one and has been evaluated *in vivo* [5,7]. Two other thermal mechanisms do not employ plasmon resonance but use gold NPs for hyperthermia treatment with radio frequency [6] and x-ray [45] excitation of thermal effects around gold NPs. These methods were realized in non-transparent animals (rats and mice), which compromised the range and control of the therapeutic effect. Furthermore, these methods require a significant amount of NPs and long excitation times (up to several minutes), and as a result cannot provide cell level selectivity, because the effects of thermal diffusion and the many NPs result in millimeter sized heated areas. The use of transparent zebrafish will improve the control of NP bio-distribution and of their optical activation in the PNB mode with cell level selectivity of the therapeutic effect.

Other agents such as gas filled, cavitation and vapor bubbles [37,39,46–57] (also including gas filled engineered micro-particles) provide diagnosis through acoustic detection, and therapy through the heat and shock waves that result from bubble collapse, such as the HIFU (high intensity focused ultrasound) method. Despite clinical trials, such bubbles do not provide either tunability or cell level selectivity. Their generation, through optical and ultrasound mechanisms, requires a prolonged treatment time (up to 6 h as compared to nanoseconds for PNB), is significantly toxic (burns, pain and other adverse effects have been reported), and depends upon additional ultrasound or magnetic resonance image guidance during the procedure. The selectivity of such bubbles is in the millimeter range and is not appropriate for the cell level. The optical generation of thermal vapor bubbles in tissue

has been employed by laser surgery at the macro- and micro-scale level for various biomedical tasks [58–63] and uses the ablative effects of laser radiation. However, laser ablation acts thermally and can not be localized to specific cells. The only exception relates to femtosecond laser intracellular surgery [64], which requires precise pointing and focusing of the laser beam into a specific area of the cell, and thus excludes clinical applications. The use of NPs as the PNB source does not require precise focusing on and pointing of the laser at the NP, yet provides the disease-specific localization of the PNB effect. The physical properties of PNBs are significantly different from those of the macro- and micro-bubbles described above for a number of vital reasons [29,32–35,43,65]. PNB is precisely tunable through plasmon excitation of gold NPs. Cell level mechanical and optical tunable effects have not been demonstrated with ultrasound-generated or any other cavitation and thermal bubbles, because such technologies cannot provide cell selectivity and localized impact. The improved bio-safety of PNBs is due to the confinement of NP-generated heat, with the temperature outside a PNB being close to the ambient level. In contrast, the generation of macro- and micro-bubbles is associated with thermal impact [66,67].

It is important to point out that PNBs, although they use the properties of both gold NPs and of the above discussed bubbles at nanoscale, are neither. PNBs are dynamically tunable, multi-functional, localized and transient (on-demand) agents, and as such represent an entirely new technology, dramatically different from any existing cellular agents. The tunability of PNBs cannot be realized in any probes whose properties are pre-determined during fabrication and cannot be changed (tuned) after they have been delivered to the target cells. To summarize, the principal benefits of PNBs compared to the aforementioned NPs and bubbles are: (1) the dynamic tuning of their function so as to support several processes with one agent: diagnosis, delivery, therapy and optical guidance of the delivery and therapy; (2) their single cell level of selectivity and specificity for diagnosis and treatment; (3) their extreme safety, since they are transient on-demand phenomena and use safe gold nanoparticles with excellent targeting properties, and do not exist until activated with an optical pulse; (4) they can be applied to treat any pathological conditions at the molecular, cellular and tissue levels with a real time adjustment of their impact and function to suit each specific situation.

Based on these results we can assume at least three modes of PNB application *in vivo* (figure 7):

1. non-invasive diagnosis: a single PNB with a lifetime below 110 ns can be detected, does not damage individual cells or tissues, and does not influence animal viability;
2. local (cell level) therapy: a single PNB with lifetimes 110–700 ns damages individual cells (where it is generated), its optical scattering signal is damage-specific although such a PNB does not disrupt tissues and does not influence animal viability;
3. tissue surgery: single or multiple PNBs with lifetimes above 700 ns disrupt the tissue and may not be safe for an animal;
4. the above specific applications can be united in one theranostic procedure: using the unique tunability feature of PNBs we can support the diagnosis, therapeutic action and the guidance of the therapeutic action in one short (about 1 μs) procedure.

The dynamic tunability of PNB is realized through real time adjustment of the energy (fluence) of the laser pulse and allows tuning of the mechanical impact and brightness of the PNB. This feature can not be supported by none of existing diagnostic and therapeutic agents.

Our recent studies of PNB have demonstrated several potential clinical applications. We were able to monitor activity of the electron transport chain in individual cells [68], PNBs successfully purified bone marrow samples by selectively killing leukemia cells [31,44] and treated a subcutaneous tumor in an animal model [30]. PNB potential for drug delivery and injection has been explored in experiments with liposomes [69]. Tissue level microsurgery has been demonstrated by recanalizing the plaque in an occluded vessel [70].

4. Conclusions

Our experiments have proved that the optical and physiological properties of zebrafish provide good conditions for precise excitation and detection of plasmonic effects *in vivo* around gold nanoparticles with nanoscale sensitivity. The systemic response of an intact organism may be very different from that observed in isolated cells. The zebrafish embryo allows testing of the response of an intact organism to complex plasmonic phenomena that involve nanoparticles, light, heat and mechanical impacts without modification of the *in vitro* methods. To compare the results observed in the zebrafish with our previous results, we generated PNBs around gold NPs in three systems: in aqueous solution, within tissue culture cells and within zebrafish embryos, using the same conditions for excitation and compared the PNBs. We observed that PNBs can be generated with the same stimulation and identical responses in all three models. The reported work has combined the unique properties of zebrafish, such as optical transparency, compatibility with gold nanoparticles and ability to deliver and collect optical radiation. To the best of our knowledge this combination has resulted in the first non-invasive application of localized plasmonic processes in zebrafish. Application of gold nanoparticles, laser radiation and the generation of plasmonic nanobubbles (including those that caused the damage at cell level) did not compromise the short term viability of zebrafish. The diagnostic mechanism of plasmonic nanobubbles is based on amplification of optical scattering and provides high sensitivity for the non-invasive and localized detection of gold nanoparticles *in vivo*. The therapeutic mechanism of plasmonic nanobubbles is based on their mechanical, nonthermal action that can be localized to individual cells and causes their damage through the immediate disruption of the target cells, while such bubbles do not damage a host (zebrafish) due to their transient and localized nature. Optical guidance of the therapeutic effect is supported by the optical scattering signal of the PNB and can be done in a real time. Finally, using dynamic tunability of the PNB we may combine the three above stages of the diagnosis, therapy and guidance of the therapy in one rapid theranostic procedure. The local nature of the PNB and their cluster-threshold mechanism of generation will provide single cell selectivity and specificity of their applications.

Acknowledgments

The authors acknowledge support from NIH 1R21CA133641, the Institute of International Education/SRF (New York, NY) (DL) and NIH R01GM77429 (DSW).

References

1. Wang H, Huff T, Zweifel D, He W, Low Wei A, Cheng J-X. Proc. Natl Acad. Sci. USA 2005;102:15752–6. [PubMed: 16239346]
2. Qian X, Peng X- H, Ansari D, Yin-Goen Q, Chen GZ, Shin DM, Yang L, Young AN, Wang MD, Nie S. Nat. Biotechnol 2008;26:83–90. [PubMed: 18157119]
3. Niidome T, Yamagata M, Okamoto Y, Akiyama Y, Takahashi H, Kawano T, Katayama Y, Niidome Y. J. Control. Release 2006;114:343–7. [PubMed: 16876898]
4. De Jong WH, Hagens WI, Krystek P, Burger MC, Sips AJAM, Geertsma RE. Biomaterials 2008;19:12–1919.

5. O'Neal DP, Hirsch LR, Halas NJ, Payne JD, West JL. Cancer Lett 2004;209:171–6. [PubMed: 15159019]
6. Cardinal J, Klune JR, Chory E, Jeyabalan G, Kanzius JS, Nalesnik M, Geller DA. Surgery 2008;144:125–32. [PubMed: 18656617]
7. Dickerson EB, Dreaden EC, Huang X, El-Sayed IH, Chu H, Pushpanketh S, McDonald JF, El-Sayed MA. Cancer Lett 2008;269:57–66. [PubMed: 18541363]
8. Zaman RT, et al. IEEE J. Sel. Top. Quantum Electron 2007;13:1715–20.
9. Chen Y-S, Hung Y-C, Liau I, Huang GS. Nanoscale Res. Lett 2009;4:858–64. [PubMed: 20596373]
10. Paciotti GF, Kingston DGI, Tamarkin L. Drug Dev. Res 2006;67:47–54.
11. Paciotti GF, Myer L, Weinreich D, Goia D, Pavel N, McLaughlin RE, Tamarkin L. Drug Deliv 2004;11:169–83. [PubMed: 15204636]
12. James WD, Hirsch LR, West JL, O'Neal PD, Payne JD. J. Radioanal. Nucl. Chem 2007;271:455–9.
13. Connor EE, Mwamuka J, Gole A, Murphy CJ, Wyatt MD. Small 2005;1:325–7. [PubMed: 17193451]
14. Shukla R, Bansal V, Chaudhary M, Basu A, Bhonde RR, Sastry M. Langmuir 2005;21:10644–54. [PubMed: 16262332]
15. Browning LM, Lee KJ, Huang T, Nallathamby PD, Lowman JE, Xu X-HN. Nanoscale 2009;1:138–52. [PubMed: 20644873]
16. Griffitt RJ, Hyndman K, Denslow ND, Barber DS. Toxicol. Sci 2009;107:404–415. [PubMed: 19073994]
17. Bar-Ilan O, Albrecht RM, Fako VE, Furgeson DY. Small 2009;5:1897–910. [PubMed: 19437466]
18. Sakakura M, Kajiyama S, Tsutsumi M, Si J, Fukusaki E, Tamaru Y, Akiyama S-I, Miura K, Hirao K, Ueda M. Japan. J. Appl. Phys 2007;46:5859–64.
19. Kohli V, Elezzabi AY. BMC Biotechnol 2008;8:7. [PubMed: 18230185]
20. Jorgensen A, Nielsen JE, Morthorst JE, Bjerregaard P, Leffers H. Reproduct. Biol. Endocrinol 2009;7:97.
21. Liu KS, Fetcho JR. Neuron 1990;23:325–35. [PubMed: 10399938]
22. Halloran MC, Sato-Maeda M, Warren JT, Su F, Lele Z, Krone PH, Kuwada JY, Shoji W. Development 2000;127:1953–60. [PubMed: 10751183]
23. Langenau DM, et al. Science 2003;299:887–90. [PubMed: 12574629]
24. Mizgireuv IV, Revskoy SY. Cancer Res 2006;66:3120–5. [PubMed: 16540662]
25. Nicol S, Ribatti D, Cotelli F, Mammalian MP. Cancer Res 2007;67:2927–31. [PubMed: 17409396]
26. Nicoli S, Presta M. Nat. Protocols 2007;2:2918–23.
27. White RM, et al. Cell Stem Cell 2008;2:183–9. [PubMed: 18371439]
28. Amatruda JF, Shepard JL, Stern HM, Zon LI. Cancer Cell 2002;1:229–31. [PubMed: 12086858]
29. Lapotko D. Opt. Express 2009;17:2538–56. [PubMed: 19219157]
30. Hleb EY, Hafner JH, Myers JN, Hanna EY, Lapotko DO. Nanomedicine 2008;3:647–67. [PubMed: 18817468]
31. Lapotko D, Lukianova E, Potapnev M, Aleinikova O, Oraevsky A. Cancer Lett 2006;239:36–45. [PubMed: 16202512]
32. Lapotko D. Int. J. Heat Mass Transfer 2009;52:1540–3.
33. Hleb EY, Hu Y, Drezek RA, Hafner JH, Lapotko DO. Nanomedicine 2008;3:797–812. [PubMed: 19025454]
34. Hleb E, Lapotko D. Nano Lett 2009;9:2160–6. [PubMed: 19374436]
35. Lapotko D. Nanomedicine 2009;4:813–45. [PubMed: 19839816]
36. Hartland G. Phys. Chem. Chem. Phys 2004;6:5263–74.
37. Vogel A, Linz N, Freidank S, Paltauf G. Phys. Rev. Lett 2008;100:038102. [PubMed: 18233040]
38. Hüttmann G, Birngruber R. IEEE J. Sel. Top. Quantum Electron 1999;5:954–62.
39. Hutson S, Ma X. Phys. Rev. Lett 2007;99:158104. [PubMed: 17995217]

40. Marston, PL. Light scattering by bubbles in liquids and its applications to physical acoustics *Sonochemistry and Sonoluminescence*. Crim, LA.; Mason, TJ.; Reisse, JL.; Suslick, KS., editors. Kluwer Academic; Dordrecht: 1999. p. 73-86.
41. Lapotko D, Kuchinsky G, Potapnev M, Pechkovsky D. Cytometry 1996;24:198–203. [PubMed: 8800552]
42. Schulte-Merker, S. Looking at embryos *Zebrafish A Practical Approach*. Oxford University Press; Oxford: 2002. p. 39-58.
43. Lapotko D, Lukianova-Hleb E, Oraevsky A. Nanomedicine 2007;2:241–53. [PubMed: 17716124]
44. Lapotko D, Lukianova E, Oraevsky A. Lasers Surg. Med 2006;38:631–42. [PubMed: 16736503]
45. Hainfield JF, Slatkin DN, Smilowitz HM. Phys. Med. Biol 2004;49:309–15.
46. Kennedy JE. Nat. Rev. Cancer 2005;5:321–7. [PubMed: 15776004]
47. Postema M, van Wamel A, Lancee C, de Jong N. Ultrasound Med. Biol 2004;30:827–40. [PubMed: 15219962]
48. Lin CP, Kelly MW. Appl. Phys. Lett 1998;72:2800–2.
49. Neumann J, Brinkmann R. J. Appl. Phys 2007;101:114701.
50. Vogel A, Noack J, Hüttmann G, Paltauf G. Appl. Phys. B 2005;81:1015–47.
51. Yao CP, Rahmanzadeh R, Endl E, Zhang ZX, Gerdes J, Hüttman G. J. Biomed. Opt 2005;10:064012. [PubMed: 16409077]
52. Stevenson D, Agate B, Tsampoula X, Fischer P, Brown CTA, Sibbett W, Riches A, Gunn-Moore F, Dholakia K. Opt. Express 2006;14:7125–33. [PubMed: 19529083]
53. Prentice P, Cuschieri A, Dholakia K, Prausnitz M, Campbell P. Nat. Phys 2005;1:107–10.
54. McDannold NJ, Vykhodtseva NI, Hynynen K. Radiology 2006;241:95–106. [PubMed: 16990673]
55. Coussio CC, Farny CH, Haar GT, Roy RA. Int. J. Hyperthermia 2007;23:105–20. [PubMed: 17578336]
56. Liu HL, Chen WS, Chen JS, Shih TC, Chen YY, Lin WL. Ultrasound Med. Biol 2006;32:759–67. [PubMed: 16677935]
57. Guzmán HR, Nguyen DX, Khan S, Prausnitz MR. J. Acoust. Soc. Am 2001;110:588–96. [PubMed: 11508983]
58. van Leeuwen TG, Meertens JH, Velema E, Post MJ, Borst C. Circulation 1993;87:1258–63. [PubMed: 8462152]
59. Prince MR, Lamuraglia GM, Seidlitz CE, Prahl SA, Athanasoulis CA, Birngruber R. IEEE J. Quantum Electron 1990;26:2297–304.
60. Proebstle TM, Lehr HA, Kargl A, Espinola-Klein C, Rother W, Bethge S, Knop J. J. Vasc. Surg 2002;4:729–36. [PubMed: 11932671]
61. van Leeuwen TG, Jansen ED, Welch AJ, Borst C. Lasers Surg. Med 1996;18:381–90. [PubMed: 8732577]
62. Brinkmann R, Hansen C, Mohrenstecher D, Scheu M, Birngruber R. IEEE J. Sel. Top. Quantum Electron 1996;2:826–35.
63. van Leeuwen TG, Jansen ED, Motamedi M, Welch AJ, Borst C. IEEE J. Quantum Electron 1994;30:1339–45.
64. Heisterkamp A, Maxwell IZ, Mazur E, Underwood JM, Nickerson JA, Kumar S, Ingber DE. Opt. Express 2005;13:3690–6. [PubMed: 16035172]
65. Lukianova-Hleb EY, Hanna E, Hafner JH, Lapotko DO. Nanotechnology 2010;21:085102.
66. Dalecki D. Annu. Rev. Biomed. Eng 2004;6:229–48. [PubMed: 15255769]
67. Matsumoto Y, Allen JS, Yoshizava S, Kaneko Y. Exp. Therm. Fluid Sci 2005;29:255–65.
68. Lapotko D, Romanovskaya T, Gordiyko E. Photochem. Photobiol 2002;75:519–26. [PubMed: 12017479]
69. Anderson LJE, Hansen E, Lukianova-Hleb EY, Hafner JH, Lapotko DO. J. Control. Release. 2010 doi:10.1016/j.jconrel.2010.02.012.
70. Hleb E, Mrochek A, Lapotko D. Lasers Surg. Med 2009;41:240–7. [PubMed: 19291755]

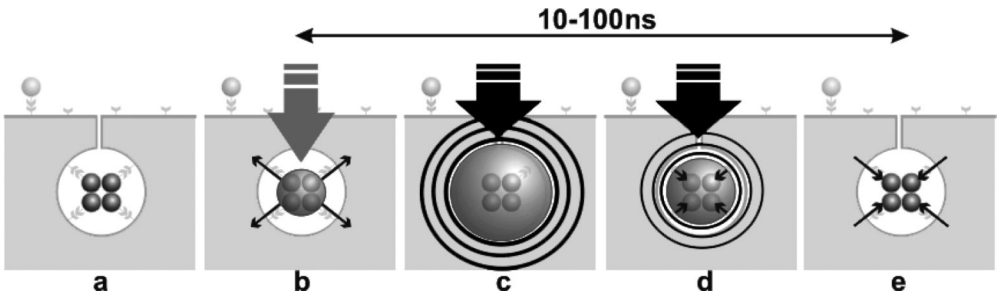

Figure 1.

The stages of transient PNB formation around gold NPs targeted to the cell (a). The pump laser pulse nucleates the PNB (b), which expands (c), thus creating mechanical impact, and then collapses (d) back to NPs (e); optical scattering of the probe laser (purple) by the PNB is amplified (c) and depends upon the PNB diameter (d), which determines the biological effect of the PNB.

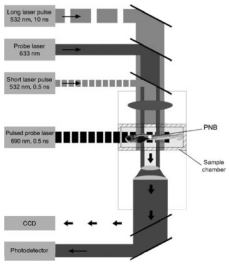

Figure 2.

Experimental setup: single gold NPs in water or individual cells in the sample chamber were mounted on the stage of an inverted optical microscope; PNB generation was provided by focused single pulses (532 nm, 0.5 ns); a pulsed probe laser (690 nm, 0.5 ns) provided time-resolved optical scattering imaging of PNBs and a continuous probe laser (633 nm, 1 mW) provided the monitoring of the integral optical scattering of PNBs though their time-responses. An additional pulsed laser (532 nm, 10 ns, 1 mJ cm^{-2}) was used for excitation of fluorescence in the cells.

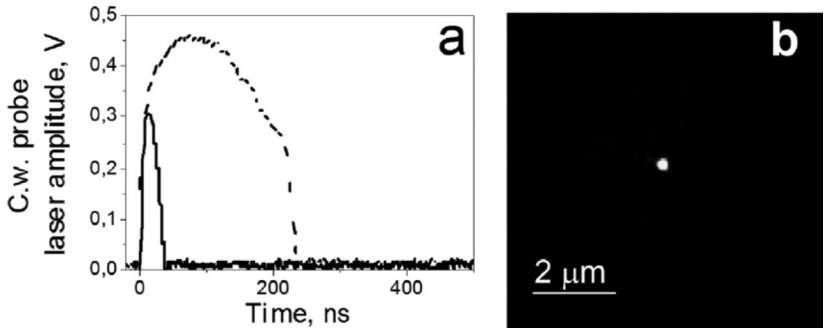

Figure 3.

Quantitative optical side scattering detection of plasmonic nanobubbles: (a) time response obtained with a continuous probe laser (633 nm), where scattering is measured with a photodetector as the electrical output (signal amplitude) for the PNB generated by a single 60 nm gold sphere (solid line) and by a cluster of the same spheres (dashed line) under identical fluence; (b) time-resolved scattering image of a single sphere-generated PNB obtained with a delay of 10 ns (relative to the pump laser pulse) pulsed probe laser (690 nm, 0.5 ns), in which the pixel amplitude is measured in counts.

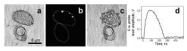

Figure 4.

In vitro generation and detection of PNB in gold NP-treated A 549 cells: (a) bright field microscopy image of two cells prior to their exposure to a single pump laser pulse (532 nm, 0.5 ns, 200 mJ cm^{-2}); (b) time-resolved scattering image of the intracellular PNBs obtained with the 10 ns delayed (relative to the pump laser pulse) pulsed probe laser (690 nm, 0.5 ns), white lines show the contours of the cells as in (a); (c) bright field microscopy image of two cells obtained 120 s after their exposure to a single pump laser pulse and the generation of the PNBs; (d) time response obtained during the exposure to a single pump laser pulse shows the bubble expansion and collapse, the baseline after the bubble collapse shows the noise of the probe laser.

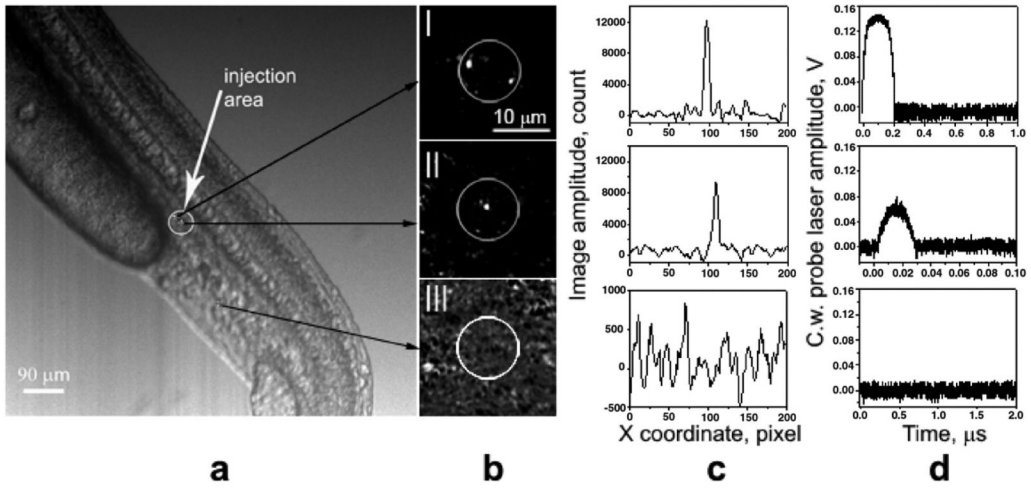

Figure 5.

(a) Bright field microscopy image of a zebrafish embryo shows the gold NP injection area (white circle) and several numbered irradiation points where single pump laser pulses were applied; (b) time-resolved scattering differential images of three numbered points obtained with the 10 ns delayed (relative to the pump laser pulse) pulsed probe laser (690 nm, 0.5 ns), the white circle shows the aperture of the pump laser beam; (c) profiles of the pixel image amplitudes for the corresponding images in (b) (1 μm is 14 pixels); (d) corresponding time response obtained during the exposure to the pump laser pulse shows the bubble expansion and collapse, the signal after the bubble collapse is identical to the baseline, note the different time (*X*) and output signal (*Y*) scales.

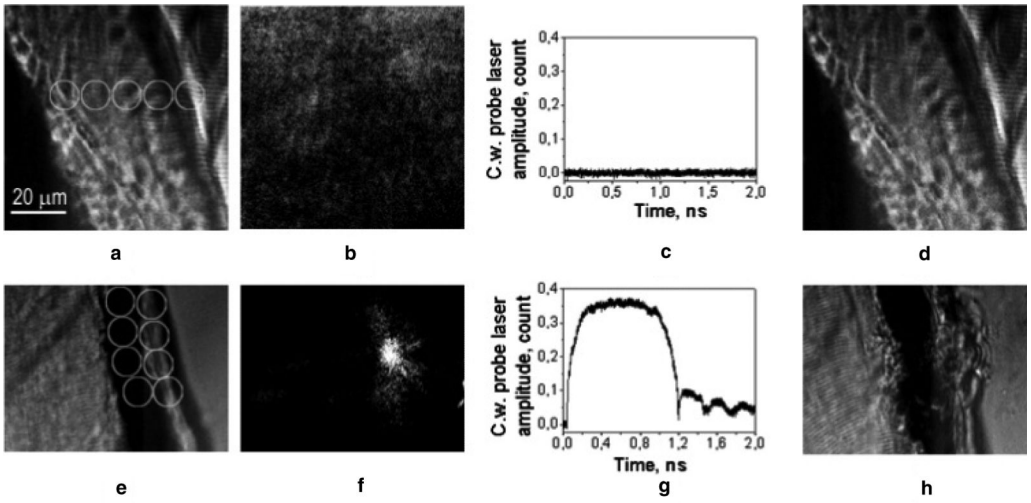

Figure 6.

(a) and (e) Bright field microscopy images of a zebrafish embryo show muscle and blood vessel areas, white circles show the areas of application of the pump laser pulses; (b) and (f) time-resolved scattering differential images of the same area obtained with the 10 ns delayed (relative to the pump laser pulse) pulsed probe laser (690 nm, 0.5 ns), white circle shows the aperture of the pump laser beam at the fluence 500 mJ cm^{-2} (b) and 740 mJ cm^{-2} (f); (c) and (g) corresponding time responses obtained during the exposure to the pump laser pulses show no bubble (c) and the bubble expansion, collapse, oscillations and residual heating after the bubble collapse (g); (d) and (h) bright field microscopy images of the same areas as in (a) and (e) obtained after their exposure to the pump laser pulses show no damage at 500 mJ cm^{-2} (d) and tissue disruption at 740 mJ cm^{-2}, white circles show the point of application of the pump laser.

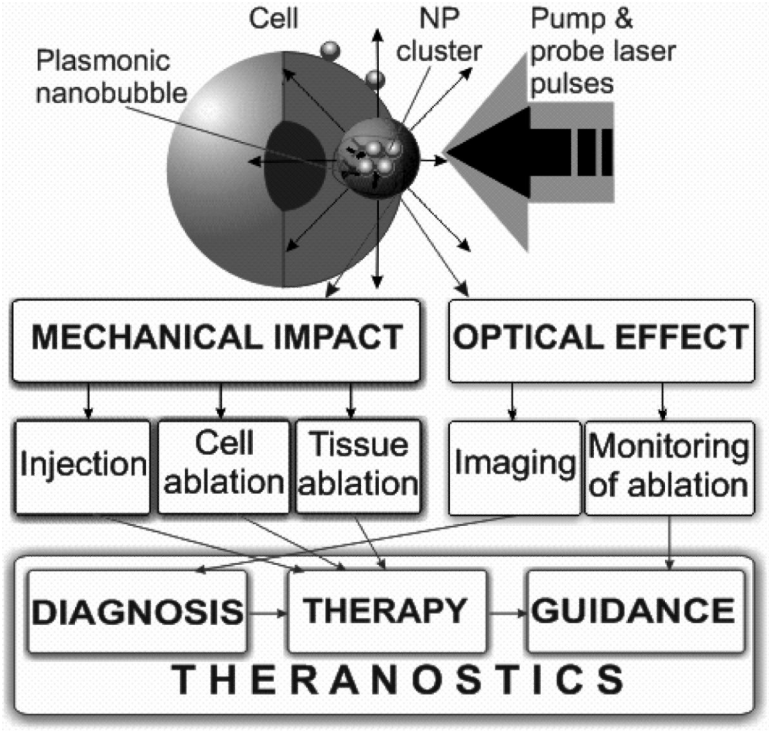

Figure 7.
Mechanisms and medical applications of PNBs for diagnosis, guided therapy and theranostics.

Table 1

PNB parameters for zebrafish, cells and gold NPs at a fluence level of the pump pulse 200 mJ cm^{-2} (532 nm, 0.5 ns, single pulse).

		Optical scattering amplitude, counts	
PNB parameter	**PNB lifetime (ns)**	**Bubble**	**Gold NP**
NP in water			
Single NPs	23 ± 13	2 500 ± 300	277 ± 49
NP clusters	125 ± 30	11 000 ± 500	600 ± 50
Cells			
NP-treated	50 ± 21	10 000 ± 455	500 ± 100
Intact	0	—	—
Zebrafish			
Point I (NP-treated, figure 5-II)	20 ± 5	9 000 ± 400	2000 ± 500
Point II (NP-treated, figure 5-I)	200 ± 25	12 000 ± 655	2000 ± 500
Point III (intact, figure 5-III)	0	—	—
Intact blood vessel	0	—	—

Table 2

Pump laser pulse fluence thresholds for bubble generation and cell damage.

Experimental parameters	Process and cell state	NP-treated cells	Untreated cells
Pump laser (532 nm, 0.5 ns)	PNB generation	0.09 ± 0.03	2.72 ± 1.8
threshold fluence (J cm^{-2})	Cell damage	1.0 ± 0.75	2.72 ± 1.8

Table 3

Viability of zebrafish as measured nine days post fertilization (dpf).

Sample	NP injection	Pump laser	PNB	Percentage of healthy zebrafish (%)	Comments
Control 1 (*n* = 9)	—	—	—	100	Intact, anesthetized and unmounted
Control 2 (*n* = 4)	—	—	—	100	Intact, anesthetized and mounted
Control 3 (*n* = 2)	+	—	—	50	Anesthetized and mounted
Test (*n* = 3)	+	+	—	100	Anesthetized and mounted, laser treatment outside injection area
Test (*n* = 2)	+	+	+	100	Anesthetized and mounted, laser treatment inside injection area